Original article
https://doi.org/10.18019/1028-4427-2025-31-3-297-306

Finite element modeling of anatomical constitutional types of the lumbar spine and pelvis (Roussouly) for study of the biomechanical aspects

A.E. Shulga✉, V.Yu. Ulyanov, Yu.Yu. Rozhkova, S.D. Shuvalov

Research Institute of Traumatology, Orthopedics and Neurosurgery
of the Saratov State Medical University named after V.I. Razumovsky, Saratov, Russian Federation

Corresponding author: Alexey E. Shulga, doc.shulga@yandex.ru

Abstract

Introduction Sagittal morphotypes graded by Roussouly are characterized by specific biomechanics of the spinopelvic alignment (SPA) that can be investigated using the finite element (FE) modeling.

The **objective** was to design three-dimensional realistic models simulating anatomical and constitutional types LPA and evaluate deformity and strength of the models under compression.

Materal and methods Lateral standing spondylograms of the skull, pelvis and upper third of the femur were produced for volunteers (n = 169) who agreed to participate in the study. Radiographs were interpreted with Surgimap 2.3.2.1.) and computed tomography (CT) of the SPA was performed for individuals (n = 5) with average sagittal parameters for each of the five Roussouly morphotypes (I, II, III, IIIA, IV). The CT findings were used to simulate (SolidWorks) five parametric finite element models of normal morphotypes of SPA and examine the deformity and strength.

Results The highest von Mises stresses under compression were measured in the bodies and intervertebral discs (IVD) ThX–LI (2.961 MPa), posterior supporting structures LIV–SI (2.515 Mpa) with type I model; vertebral bodies and IVD of the thoracic and lumbar spine, mainly at the ThXII–LI (3.082 MPa) and LIV–LV (3.120 Mpa) levels with type II model; anterior aspects of the bodies and IVD ThXI–LII, posterior thirds of the bodies, pedicles and facet joints LI–SI (1.720 Mpa) with type III model; the bodies and intervertebral discs of the ThIX–LII vertebrae (1.811 MPa), posterior supporting structures of the LI–SI vertebrae (1.650 Mpa) with type IIIA model; in the spinous processes and articular portion of the arches of the LI–SI vertebrae (3.232 MPa) with type IV model.

Discussion The lateral configuration of the SPA has a key effect on the segmental distribution of gravitational force and determines the specificity of the sagittal biomechanics of the spine, its resistance to dynamic loads and tendency to various degenerative pathologies.

Conclusion Types III and IIIA were the most biomechanically balanced types, hypolordotic form (types I and II) was associated with overloaded anterior vertebral structures including intervertebral disc protrusion (IDP) and overloaded posterior supporting structures in case of hyperlordosis (type IV).

Keywords: spine, sagittal balance, Roussouly classification, mathematical modeling, finite element analysis

For citation: Shulga AE, Ulyanov VYu, Rozhkova YuYu, Shuvalov SD. Finite element modeling of anatomical constitutional types of the lumbar spine and pelvis (Roussouly) for study of the biomechanical aspects. *Genij Ortopedii*. 2025;31(3):297-306. doi: 10.18019/1028-4427-2025-31-3-297-306.

INTRODUCTION

The human vertebral column became S-shaped during evolution which is optimal for maintaining an economical orthostatic position [1, 2]. The geometric combination of the physiological curvatures and the pelvis provides a balance chain with the coordination proportionally distributing the trunk weight around the gravitational line minimizing energy expenditures and the need for conscious postural control [3].

In 1992, Duval-Beaupere et al. introduced the concept of sagittal balance and described a number of radiometric parameters of the pelvis, emphasizing the role of morphology in the regulation of postural balance [4]. Studies of the profile geometry of the spinopelvic complex (SPC) revealed significant anatomical variability of the spine in healthy individuals and the impossibility of systematizing the sagittal shape based on average radiometric parameters [5]. In 2005, Roussouly offered to distinguish four morphological types of the SPC in the normal population considering the sacral slope and the sagittal shape of the spine [6]. A hypothesis was proposed about the type-specificity of the distribution of gravitational load on various vertebral structures, which implies the presence of sagittal biomechanics and degeneration of the SPC, being characteristic of each of its morphotypes [7].

The conclusions are mostly based on the analysis of radiometric parameters and are of an inferential nature [8]. Fundamental research is aimed at objectifying the causes of various spinal conditions [9]. Finite element (FE) analysis is one of the most popular methods to simulate a real physical system (geometry and loading conditions) using mathematical approximation [10]. Simple and interacting elements (units) are used with a finite number to be employed for approximation of a real system with an infinite number of unknowns [11]. The FE modeling is widely used in clinical studies due to the reproducibility of its results and low cost of the experiment [12]. FE analysis can be practical for the study of the etiology of degenerative diseases of the spine and for identification of various factors affecting lumbar biomechanics, including the geometric variability of morphotypes of the SPC [13].

Understanding of the sagittal biomechanics of the morphological types of SPC is important for the study of the pathogenesis of degenerative spine diseases to predict outcomes of surgical interventions.

The **objective** was to design three-dimensional realistic models simulating anatomical and constitutional types of SPA and evaluate deformity and strength of the models under compression.

MATERIAL AND METHODS

The FE model of the spine was constructed based on the model proposed by Kolmakova and Rikun [14]. Lordosis and kyphosis are associated with different intervertebral heights anteriorly and posteriorly where the intervertebral disc (IVD) is located. The IVD consists of cartilaginous tissue and is anatomically divided into three parts. The inner part (nucleus pulposus) is a gel-like mass rich in water. The outer portion (fibrous ring) has a hard and fibrous structure. The third part of the disc is a thin layer of hyaline cartilage, which separates the disc from the vertebral body. The geometric model includes the CIII (1) and CIV (2) vertebrae, the intervertebral disc (3), facet joints (4), the interspinous ligament (5), the posterior vertebral arches (6), the spinous (7), transverse (8), and articular (9) processes (Fig. 1 a). Cancellous (10) and compact bone tissue are present in the vertebrae (Fig. 1 b).

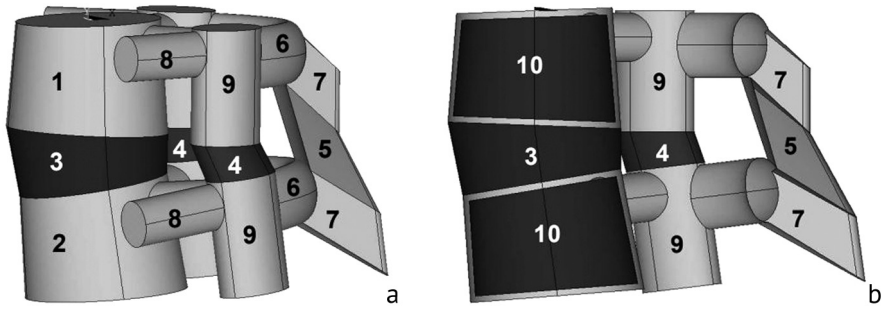

Fig. 1 Geometric model of the CIII–CIV segment of the cervical spine: (a) isometric view; (b) sectioned lateral view [14]

A thin cortical layer covers vertebral bodies. It is assumed that simulated vertebral arches and vertebral processes consist of compact bone tissue. The Z-axis of the coordinate system is directed along the segment axis. The X-axis is directed in the anteroposterior direction of the spinal segment. The presence of lordosis is considered due to a greater anterior IVD height, or kyphosis with a lower anterior height of the disc.

The geometric model of segments with different geometric parameters was used for FE modeling and determination of the stress-strain in the thoracic (ThI–ThXII) and lumbar (LI–LV) spine.

The bone components and intervertebral discs were integrated using first-order hexahedral hybrid solid FEs. The collagen fibers of the annulus and ligaments were represented by flat truss FEs (T2D2). The facet joint surfaces were modeled using frictionless surface-to-surface contact. The nucleus pulposus (NP) and the annular matrix were considered as a virtually incompressible hyperelastic material as described by the Mooney-Rivlin law.

Young's modulus for NP was measured in the range of 0.0045–1.5 MPa ($\nu = 0.45$) and 20 MPa ($\nu = 0.4$) for hyaline plates. The deformed collagen fibers were described by a nonlinear stress-strain function. The contact between the surfaces of the facet joints was assumed to be rigid with a friction coefficient of 0.15. The layers of facet cartilage with an initial gap of 0.5 mm were described as elastically isotropic (Young's modulus 35 MPa).

Cortical and cancellous bone tissues of the vertebral bodies, IVD, facet joints, interspinous ligaments, vertebral arches and processes were considered to be isotropic linearly elastic materials. The mechanical characteristics of the structural components of the segments were set in accordance with the literature data [15, 16] (Table 1).

Table 1

Mechanical properties of the structural components of the vertebral segment

Structural component	Young's modulus of elasticity, MPa	Poisson's ratio
Cortical bone	10000	0.3
Cancellous bone	100	0.2
Facet joints	1,5	0.3
Intervertebral disc	2,5–98	0.45
Interspinous ligament	3,5	0.3

Young's modulus of elasticity and Poisson's ratio for the structural components of the spine were presented in different ranges [6]. The calculations were produced using the ABAQUS software package using the finite element method; the problem was solved using the linear theory of elasticity. Geometric models were constructed in accordance with the actual dimensions of the cervical [17], thoracic, lumbar [18] spine and intervertebral disc [19].

Based on the conducted research, the following sequence of steps was proposed for implementing the algorithm for modeling the stress-strain of the spinal elements:

1) determination of the initial reference body geometry for calculations of the spine (the body relative to which the position of a given body is determined);
2) determination of the displacement of segments for each type of spinal column relative to the position of the segments in the reference body according to the projection of the spine onto the vertical plane;
3) division of the spinal column segment system into sections to be used in the ABAQUS program to form finite superelements used to reduce the amount of calculations in the FE method;
4) Numerical solution for determining the stress-strain of the spinal column in the displacements defined in paragraph 2;
5) determination of additional equivalent stresses in the spinal segments caused by displacements relative to the reference body.

Mesh Convergence Study

A linear hexahedral mesh and eight-node quadratic tetrahedral elements (C3D8) were considered for the cortical bone, cancellous bone, and posterior supporting structures. Collagen fibers of the annulus and ligaments were represented by plane truss elements (T2D2). A mesh convergence test was performed to determine the appropriate mesh resolution of the FE model to confirm the accuracy of the simulation. The mesh density was found to provide good convergence of results with an element side length of approximately 1–1.5 mm. The mesh convergence results showed a difference of less than 5 % in the IVD loads when the number of elements was doubled.

Screening of the healthy population was produced to select individuals with different sagittal morphology of the spine in accordance with the classification revised by Roussouly (2017) [20]. Lateral standing spondylograms of the skull, pelvis and upper third of the femur were produced for volunteers who agreed to participate in the study. Sagittal parameters of the SPC (Surgimap 2.3.2.1.) were interpreted and the subject was assigned to one of the five Roussouly types. Finally, 169 volunteers were rated as type I (n = 20; 11.9 %), type II (n = 42; 24.9 %), type III (n = 50; 29.6 %); type IIIA (n = 25; 14.7 %), type IV (n = 32; 18.9 %). The number of patients in each group was averaged to 20 to improve the proportionality of the data.

The resulting database of 100 individuals allowed us to determine the normal ranges of sagittal parameters (Sacral Slope, SS; Pelvic Incidence, PI; Pelvic Tilt, PT; Global Lumbar Lordosis, GLL; Lordosis Tilt Angle, LTA; Lumbar Lordosis Apex, LLA; Number (verteb) Lumbar Lordosis, NLL) for each of the five morphotypes. The radiographic parameters were subjected to standard statistical analysis, which showed a normal distribution of the variables in the study population. Parametric statistics methods were used for calculations, and quantitative parameters were presented as the arithmetic mean and standard deviation (Table 2). The arithmetic mean values of all radiometric sagittal parameters were measured in each of the five groups characterizing the “reference” lateral shape of the SPC for a specific group, and the standard deviation allowed geometric variations of morphotypes within the designated boundaries. The selected volunteers underwent computed tomography (CT) of the SPC for modeling of parametric FE models.

Table 2

Mean values of sagittal parameters for different Roussouly morphotypes (n = 100), descriptive statistics

Roussouly type	n valid (by list)	Parameters							
		Statistical indicator	age	PI	SS	PT	GLL	LTA	LLA	NLL
I	20	$\bar{X}$	40.70	38.845	29.450	10.110	−50.295	−7.930	5.375	2.650
		σ	6.697	3.6176	2.7907	2.9693	4.2201	2.3595	0.2221	0.4894
II	20	$\bar{X}$	39.40	40.765	30.830	10.270	−48.080	−5.910	4.225	4.075
		σ	6.916	4.3347	2.9631	2.7741	4.3819	1.5697	0.2552	0.5200
III	20	$\bar{X}$	40.30	52.955	39.855	13.080	−59.395	−3.950	4.250	4.100
		σ	7.420	3.5798	2.0028	3.2638	3.6360	2.6106	0.3804	0.5282
IIIA	20	$\bar{X}$	38.85	48.140	45.140	4.140	−64.525	−5.495	4.100	4.775
		σ	8.768	3.0285	4.5217	1.9228	4.3052	2.1852	0.5982	0.2552
IV	20	$\bar{X}$	39.90	62.270	49.850	12.045	−70.555	−1.530	3.175	5.650
		σ	7.752	3.8674	2.8057	4.1461	4.0028	2.1436	0.2447	0.5155

Note: $\bar{X}$ — arithmetic mean; σ — standard deviation.

RESULTS

Parametric FE models were developed in the SolidWorks environment to explore deformation and strength properties of five normal morphotypes of the SPC in accordance with the revised classification of Roussouly. Computer tomograms of five "reference" volunteers selected at the previous stages of the study were used as input data for modeling the spine. The models were constructed in accordance with the determinants of sagittal morphology of the STC, determined by Roussouly for each of the five morphotypes [20], and the radiometric parameters of the “reference” participants.

The simulated three-dimensional model type I (Fig. 2 a) was characterized by low-grade SS (29.4°) and PI (39.4°), had a short (NLL, 3 vertebrae) lumbar hyperlordosis (GLL, (–49.5°)) with a low location of the apex (LLA, IVD LIV–LV) and a negative LTA value (–8.9°). The thoracolumbar spine was characterized by an extended kyphosis, and the PT value (10.3°) corresponded to the average values of the normal range (0–20°).

Type II (Fig. 2 b) was characterized by low-grade values of SS (31.3°) and PI (41.2°). The model was constructed taking into account the hypolordoticity (GLL, (–47.9°)) and hypokyphoticity of the spinal column and in accordance with a higher (than in type I) location of the LLA (the center of the LIV vertebra), a more positive LTA (–6.7°), a larger number of vertebrae in the lordotic arch (NLL, 4 vertebrae) and average PT values (9.8°).

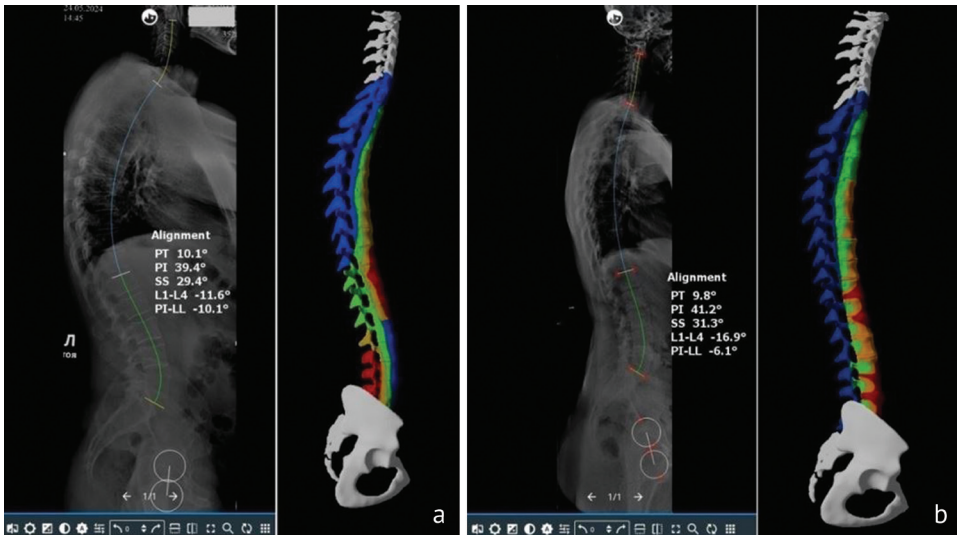

Fig. 2 Sagittal parameters (Surgimap 2.3.2.1.) measured in (a) a volunteer with type I SPC; (b) participants with type II SPC and a 3D model

Three-dimensional modeling of morphotype III (Fig. 3 a) involved the radiometric parameters of the corresponding "reference" participant as SS (39.6°), PI (52.2°), and GLL (–58.8°). This variant of the geometric shape was characterized by a relatively long arc of the lumbar lordosis (NLL, 4.5 vertebrae), high position of the LLA (LPD LIII–LIV), lower LTA values (–4.5°), and average PT values (12.6°).

Some of the parameters used to model type IIIA (Fig. 3 b) were comparable with those used for morphological type III (LTA, –6.1°; LLA, IVD LIII–LIV; NLL, 5 vertebrae), but a number of criteria had differences characteristic of this morphotype. The pelvic anteversion PT (3.9°) specific to type IIIA determined a combination of high SS (45.0°) and GLL (–65.0°) values with low PI parameters (48.9°).

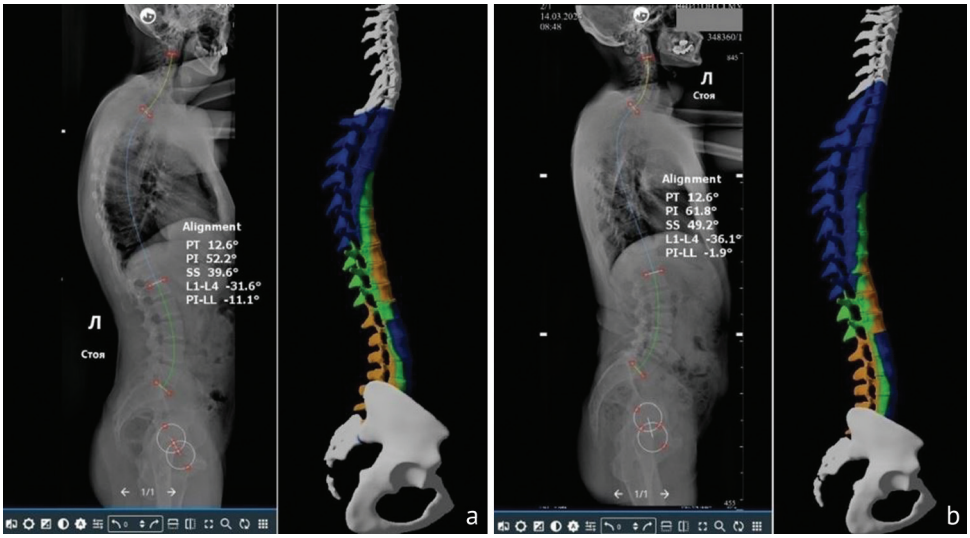

Fig. 3 Sagittal parameters (Surgimap 2.3.2.1.) measured in (a) a volunteer with SPC type III; (b) a volunteer with SPC type IIIA and a 3D model

The three-dimensional model of type IV (Fig. 4) was represented by a harmonious hypercurved SPC with segmental hyperextension of the lumbar spine. The large PI value (61.8°), characteristic of this sagittal morphotype, served as a determinant of a large sacral slope SS (49.2°) and a high-grade GLL (–69.8°), extended LLA (MPD L2–L3; NLL, 5.5 vertebrae) of lumbar lordosis.

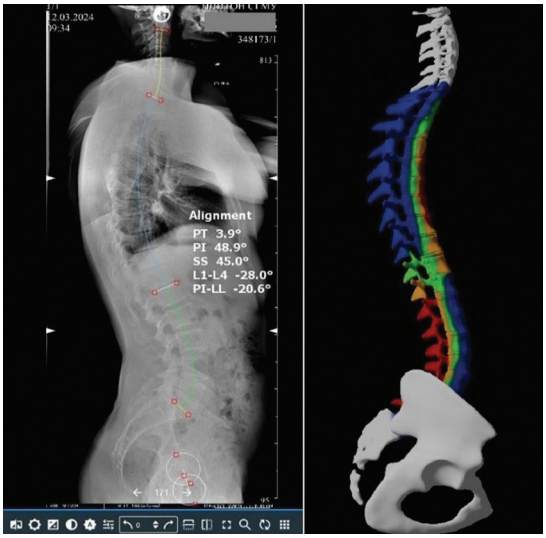

Fig. 4 Sagittal parameters (Surgimap 2.3.2.1.) measured in a volunteer with SPC type IV and a 3D model

LTA (–1.8°) was characterized by values close to 0, and PT (12.6°) was within the average values of the normal range (0–20°).

The FE models of Roussouly five sagittal types of SPC allowed us to explore and characterize the stress-strain state under axial load. All nodes of the lower surface of the FE model of the LV vertebra were fixed as boundary conditions.

Color maps of the stress-strain of five vertebral morphotypes were determined with the FE method. Various zones of the stress-strain of the vertebrae were determined using the results of the method offered to 3D models of the spinal column: the red color corresponded to the zone of the maximum stress; the blue color characterized the minimum vertebral stress; the color transition indicated the stress effect on the adjacent vertebrae.

The type I model showed the highest von Mises equivalent stresses in the thoracolumbar region under axial load (Fig. 2 a). The bodies and IVDs of the ThX–LI vertebrae were the most heavily loaded parts (2.961 MPa). The highest stresses occurred on the posterior supporting structures (spinous processes, articular processes, pedicles) of the lumbar spine and on the dorsal part of the bodies of the lower lumbar vertebrae (LIV–SI) (2.515 Mpa).

The type II model demonstrated the highest equivalent stresses in the anterior supporting structures (vertebral bodies and IVD) of the thoracic and lumbar spine under compression load (Fig. 2 b). The stress field was uneven throughout the specified region, with the highest values noted at the ThXII–LI (3.082 MPa) and LIV–LV (3.120 MPa) levels. The posterior supporting structures of the second type of the spine experienced insignificant loads (0.650 MPa).

The third type, due to its geometric balance, was characterized by biomechanical stability (Fig. 3 a). The most loaded zone was noted in the anterior thoracolumbar vertebrae and IVD (ThXI–LII) and along the lumbar spine (LI–SI): mainly the posterior third of the vertebral bodies, the pedicles and facet joints (1.720 MPa). Nevertheless, the stress level was characterized by significantly lower values compared to Roussouly morphotypes I and II (1.431 Mpa).

The increased stress level in type IIIA had a localization characteristic of type III, but was characterized by a greater extent of boundaries (Fig. 3 b). It covered the area from ThIX to LII vertebrae, and extended to the posterior sections of the bodies of LIII–LV vertebrae. The stresses exceeded those in type III, both in the thoracic (1.811 MPa) and lumbar spine (1.650 Mpa).

The type IV model demonstrated the biomechanics of a hypercurved vertebral column (Fig. 4). In the thoracic region, zones with a moderate level of equivalent stresses (2.743 MPa) were identified along the anterior surface of the bodies (anterior half of the bodies and IVD) of the ThIII–ThXI vertebrae under axial loads. The posterior supporting structures of the LI–SI vertebrae was found to be the most heavily loaded, while the stress values on the spinous processes and articular sections of the arches had values similar to those of type I (3.232 MPa).

DISCUSSION

In recent decades, significant progress has been noted in the study of sagittal morphology and biomechanics of the SPC with assessments becoming a routine procedure in the diagnosis and treatment of various spinal conditions [21]. The variability of the profile geometry of the SPC in healthy individuals was reported by several researchers with the presence of four types (with a fifth subtype in the revised classification) of the normal profile configuration substantiated and the type-specificity of diseases proven. Reproducible and accessible methods for modeling the spinal column are used to objectify the causes of the degenerative pathology [22]. FE modeling is the most common method for studying the spine biomechanics *in silico* [23]. The results of various tests conducted on mathematical models of the spinal column are published to confirm the conclusions of analytical studies [24, 25].

In the present experiment, an attempt was made to explore the mechanical characteristics of parametric FE models of four classical types of SPC and the retroverted variant of morphotype III, constructed on the basis of CT scans of the spine of healthy subjects with average values of sagittal parameters. The findings demonstrated a significant influence of the profile configuration of five SPC models on their sagittal biomechanics, which was manifested by different reactivity of the FE stiffness matrix under axial compression load. The data on the stress-strain of the models confirmed the theoretical patterns formulated earlier in the majority of cases [7]. The hypolordotic lumbar spine was considered as the main predictor of IVD degeneration considering the concept of "contact force" presented by Roussouly. Subsequent clinical studies have repeatedly confirmed the fact that individuals with discogenic pathology are characterized by low PI values corresponding to hypolordosis [26, 27]. The deformation and strength properties of FE models with low PI (types I and II) indicated zones of the greatest equivalent stresses in the vertebral bodies and IVD, mainly in the thoracolumbar (type I, ThX–LI; type II ThXII–LI) and lumbar (type I, LIV–SI; type II LIV–LV) spine. With the vertebral endplates oriented in a plane being closer to the horizontal plane the gravitational load vector has perpendicular impact on them increasing the overload of the IVD. There are significant stresses on the posterior supporting structures (spinous processes, articular processes, pedicles) in the FE model of type I. These features are caused by a short hypercurved lordosis, when the vector of biomechanical axial action is shifted to the posterior supporting column. There are data in the literature that are consistent with our findings. Müller et al. reported complex loads on 28 FE models of the lumbar spine and indicated the compression force had impact primarily on the IVD with a hypolordotic lumbar spine, and on the contrary, the facet joints were more susceptible to its influence with high LL values [28]. The significant impact of gravitational load on the posterior supporting structures of the lumbar spine under hyperlordosis conditions was confirmed by out findings in the study of the stress-strain condition of the FE model of morphotype IV. In addition to that, the region of increased equivalent stresses of this model was determined in the bodies and IVD at the level of thoracic hyperkyphosis (ThIII–ThXI). Roussouly et al. interpreted the biomechanics of local stresses of the hypercurved lumbar spine and noted that the distribution of the KS depended on the PI value [7]. The higher the PI values, the more inclined are the vertebrae that make up the lower arc of the lumbar lordosis, that contributes to the distribution of the gravitational load parallel to the endplates. Under these conditions, the pressure on the IVD decreases, and the facet joints are subject to a combined effect of axial (due to hyperextension) and shear (due to sliding force). The study of FE models of types III and IIIA showed no zones of mechanical overloads equivalent to types I, II and IV, which characterizes their geometric balance and biomechanical harmony. Moderate stress zones in type III and type IIIA were localized in the bodies and IVDs of the thoracolumbar spine, on the posterior supporting structures of the lumbar spine of the FE models. There are similar studies assessing stresses and resulting deformations along the spinal column using geometrically personalized FE models. The authors came to the conclusion that the PI value was closely related to the distribution of load forces: the stress is distributed evenly along the entire spine with the hypolordotic form; the load concentration is observed mainly around the lower part of the spinal column (LIII–LV) with the normal and hyperlordotic configuration [29, 30].

The profile configuration of the SPC has a substantial influence on the segmental distribution of gravitational force and determines the specificity of the sagittal biomechanics of the spine, the resistance to dynamic loads and susceptibility to various degenerative conditions. Type III and type IIIA appeared to be the most balanced types, the anterior vertebral structures including the IVD were overloaded with the hypolordotic form (types I and II), and the posterior supporting structures were overloaded in the case of hyperlordosis (type IV) or local hyperextension (type I).

CONCLUSION

The FE modeling algorithm offered allows *in silico* estimation of the stress-strain condition of various spinal structures with high reproducibility of results. The FE analysis of three-dimensional realistic models of the spinal column, constructed using the geometric parameters of Roussouly five morphological types demonstrated the ambiguity of the sagittal biomechanics. Morphotypes III and IIIA demonstrated the most harmonious distribution of equivalent stresses, whereas hypo- (types I and II) and hyperlordotic (type IV) forms of SPC contributed to type-specific overload of various parts of the spine. Therefore, the anatomical and constitutional features of the spinal column can be considered one of the main factors determining the resistance to dynamic loads and its tendency to different degenerative conditions.

Conflicting Interests *The authors declared no potential conflicts of interest with respect to the authorship and/or publication of this article.*

Informed Consent *Informed consent was obtained from all patients for being included in the study.*

REFERENCES

1. Diebo BG, Varghese JJ, Lafage R, et al. Sagittal alignment of the spine: What do you need to know? *Clin Neurol Neurosurg*. 2015;139:295-301. doi: 10.1016/j.clineuro.2015.10.024.
2. Le Huec JC, Saddiki R, Franke J, et al. Equilibrium of the human body and the gravity line: the basics. *Eur Spine J*. 2011;20(Suppl 5):558-563. doi: 10.1007/s00586-011-1939-7.
3. Hasegawa K, Okamoto M, Hatsushikano S, et al. Standing sagittal alignment of the whole axial skeleton with reference to the gravity line in humans. *J Anat*. 2017;230(5):619-630. doi: 10.1111/joa.12586.
4. Duval-Beaupère G, Schmidt C, Cosson P. A Barycentremetric study of the sagittal shape of spine and pelvis: the conditions required for an economic standing position. *Ann Biomed Eng*. 1992;20(4):451-62. doi: 10.1007/BF02368136.
5. Berthonnaud E, Dimnet J, Roussouly P, Labelle H. Analysis of the sagittal balance of the spine and pelvis using shape and orientation parameters. *J Spinal Disord Tech*. 2005;18(1):40-47. doi: 10.1097/01.bsd.0000117542.88865.77.
6. Roussouly P, Gollogly S, Berthonnaud E, Dimnet J. Classification of the normal variation in the sagittal alignment of the human lumbar spine and pelvis in the standing position. *Spine (Phila Pa 1976)*. 2005;30(3):346-53. doi: 10.1097/01.brs.0000152379.54463.65.
7. Roussouly P, Pinheiro-Franco JL. Biomechanical analysis of the spino-pelvic organization and adaptation in pathology. *Eur Spine J*. 2011;20 Suppl 5(Suppl 5):609-18. doi: 10.1007/s00586-011-1928-x.
8. Naoum S, Vasiliadis AV, Koutserimpas C, et al. Finite Element Method for the Evaluation of the Human Spine: A Literature Overview. *J Funct Biomater*. 2021;12(3):43. doi: 10.3390/jfb12030043.
9. Kossovich LYu, Kharlamov AV, Lysunkina YuV, Shul'ga AE. Mathematical modeling and prediction of the effectiveness of surgical treatment in surgery of the spine and pelvic complex. *J Samara State Tech Univ Ser Phys Math Sci*. 2019;23(4):744-755. doi: https://doi.org/10.14498/vsgtu1702.
10. Zhang S, Bai T, Zhang X, et al. Application of Finite Element Analysis in Biomechanical Research of Degenerative Diseases of Lumbar Spine. *JBM*. 2022;(10):21-33. doi: 10.4236/jbm.2022.103004.
11. Kudo N, Yamada Y, Xiang X, et al. Concept of mathematical modeling of lumbar and thoracic spine based on elastic beam theory. *JBSE*. 2022;17(2):21-00331. doi: 10.1299/jbse.21-00331.
12. Sciortino V, Pasta S, Ingrassia T, Cerniglia D. On the Finite Element Modeling of the Lumbar Spine: A Schematic Review. *Appl Sci*. 2023;13(2):958. doi:10.3390/app13020958.
13. Cho PG, Yoon SJ, Shin DA, Chang MC. Finite Element Analysis of Stress Distribution and Range of Motion in Discogenic Back Pain. *Neurospine*. 2024;21(2):536-543. doi: 10.14245/ns.2347216.608.
14. Kolmakova TV, Rikun YuA. Study of deformation behavior of the intervertebral disc with the slope of cervical spine segment. *Bulletin of the Buryat State University: Mathematics, informatics*. 2017;(2):54-60. (In Russ.)
15. Grigoriev AI, Volozhin AI, Stupakov GP. Mineral metabolism in humans under conditions of altered gravity. In: *Problems of space biology*. Moscow: Nauka Publ.; 1994. 994;74:192-212. (In Russ.)
16. Berezovsky VA, Kolotilov NN. *Biophysical characteristics of human tissues: reference book*. Kiev: Nauk. Dumka; 1990:224. (In Russ.)
17. Chumachenko EN, Logashina IV. Calculation of the stress-strain state of the spinal motor segment under loads. *Aerospace and Environmental Medicine*. 2014;48(5):51-57. (In Russ.)
18. Tan SH, Teo EC, Chua HC. Quantitative three-dimensional anatomy of cervical, thoracic and lumbar vertebrae of Chinese Singaporeans. *Eur Spine J*. 2004;13(2):137-146. doi: 10.1007/s00586-003-0586-z.
19. Berry JL, Moran JM, Berg WS, Steffee AD. A morphometric study of human lumbar and selected thoracic vertebrae. *Spine (Phila Pa 1976)*. 1987;12(4):362-367. doi: 10.1097/00007632-198705000-00010.
20. Laouissat F, Sebaaly A, Gehrchen M, Roussouly P. Classification of normal sagittal spine alignment: refounding the Roussouly classification. *Eur Spine J*. 2018;27(8):2002-2011. doi: 10.1007/s00586-017-5111-x.
21. Abelin-Genevois K. Sagittal balance of the spine. *Orthop Traumatol Surg Res*. 2021;107(1S):102769. doi: 10.1016/j.otsr.2020.102769.
22. Galbusera F, Brayda-Bruno M, Costa F, Wilke HJ. Numerical evaluation of the correlation between the normal variation in the sagittal alignment of the lumbar spine and the spinal loads. *J Orthop Res*. 2014;32(4):537-544. doi: 10.1002/jor.22569.

23. Wang W, Pei B, Wu S, et al. Biomechanical responses of human lumbar spine and pelvis according to the Roussouly classification. *PLoS One*. 2022;17(7):e0266954. doi: 10.1371/journal.pone.0266954.
24. Bassani T, Casaroli G, Galbusera F. Dependence of lumbar loads on spinopelvic sagittal alignment: An evaluation based on musculoskeletal modeling. *PLoS One*. 2019;14(3):e0207997. doi: 10.1371/journal.pone.0207997.
25. Remus R, Selkmann S, Lipphaus A, et al. Muscle-driven forward dynamic active hybrid model of the lumbosacral spine: combined FEM and multibody simulation. *Front Bioeng Biotechnol*. 2023;11:1223007. doi: 10.3389/fbioe.2023.1223007.
26. Cosgun Z, Dagistan E, Dagistan Y. Effects of sagittal balance differences on spondylolisthesis. *Acta Ortop Bras*. 2019;27(2):120-123. doi: 10.1590/1413-785220192702205665.
27. Yüksel S, Özmen E, Barış A, et al. Publication Trends in the Pelvic Parameter Related Literature between 1992 and 2022 : A Bibliometric Review. *J Korean Neurosurg Soc*. 2024;67(1):50-59. doi: 10.3340/jkns.2023.0047.
28. Müller A, Rockenfeller R, Damm N, et al. Load Distribution in the Lumbar Spine During Modeled Compression Depends on Lordosis. *Front Bioeng Biotechnol*. 2021;9:661258. doi: 10.3389/fbioe.2021.661258.
29. Naserkhaki S, Jaremko JL, El-Rich M. Effects of inter-individual lumbar spine geometry variation on load-sharing: Geometrically personalized Finite Element study. *J Biomech*. 2016;49(13):2909-2917. doi: 10.1016/j.jbiomech.2016.06.032.
30. Filardi V, Simona P, Cacciola G, et al. Finite element analysis of sagittal balance in different morphotype: Forces and resulting strain in pelvis and spine. *J Orthop*. 2017;14(2):268-275. doi: 10.1016/j.jor.2017.03.007.

The article was submitted 09.01.2025; approved after reviewing 18.02.2025; accepted for publication 31.03.2025.

Information about authors:

Alexey E. Shulga — Candidate of Medical Sciences, Research Fellow,
doc.shulga@yandex.ru, https://orcid.org/0000-0001-8476-0231;

Vladimir Yu. Ulyanov — Doctor of Medical Sciences, Deputy Director, Assistant Professor,
v.u.ulyanov@gmail.com, https://orcid.org/0000-0002-9466-8348;

Yuliya Yu. Rozhkova — Head of Department, rozhkova280586@gmail.com, https://orcid.org/0000-0001-9506-5234;

Stanislav D. Shuvalov — Neurosurgeon, shuvalov.stan@yandex.ru, https://orcid.org/0000-0002-8095-9398.